

# Data-driven Modeling of Linearizable Power Flow for Large-scale Grid Topology Optimization

Young-ho Cho, *Student Member, IEEE*, and Hao Zhu, *Senior Member, IEEE*

**Abstract**—Effective power flow (PF) modeling critically affects the solution accuracy and computation complexity of large-scale grid optimization problems. Especially for grid optimization with varying topologies for enhanced flexibility and resilience, a tractable approximation of nonlinear AC-PF is of paramount importance. This work develops a data-driven approach to obtain piecewise linear (PWL) PF models by using the ReLU activation and an innovative neural network (NN) layer design to match the generative structure of AC-PF models like nodal power balance. Accordingly, the proposed generative NN (GenNN) PF model not only maintains the consistency among the predicted power variables but also neatly includes the topology decision variables for attaining a mixed-integer linear program (MILP) based reformulation of grid topology optimization problems. We further develop an area-partitioning based sparsification method to reduce the number of GenNN weight parameters and thus the model complexity. Thanks to our sparse GenNN, the proposed PWL-PF can achieve scalability for large-scale systems and allow for efficient solutions of AC-PF based optimal transmission switching (OTS) and restoration order problems (ROP). Numerical tests on the IEEE 118-bus and the 6716-bus synthetic Texas grid systems have demonstrated performance improvements over competing alternatives in approximating the AC-PF and accelerating topology optimization solutions.

## I. INTRODUCTION

**P**OWER flow (PF) modeling is an essential power system analysis task for attaining efficient and reliable grid operations. With the trend in energy decarbonization, solving grid optimization is significant for enhancing the flexibility and resilience of power grids under uncertain and extreme operating conditions. The nonlinearity of AC-PF equations greatly challenges various grid optimization tasks such as the well-known optimal power flow (OPF). Recent interest in the optimal transmission switching (OTS) [1] and restoration ordering problem (ROP) [2] for enhanced resilience further increases the complexity of grid optimization due to the integer topology variables therein. Hence, an accurate yet tractable approximation of the nonlinear PF model can improve the optimality and computation time of grid optimization problems, especially those with combinatorial topology variables.

Developing PF approximation models has been an active research area. Notably, linearized power flow models have been advocated for their simplicity, such as the well-known DC model [3] and the more general first-order approximation at a given operating point for improved accuracy [4]. However, linear models are very limited in their generalizability

across all possible operating conditions [5]. A straightforward extension is the piecewise linear (PWL) approximation, which utilizes multiple operating points for linearization; see e.g., [6]. There is a trade-off between accuracy and complexity in these model-based approaches, and the best number and location of operating points can be difficult to determine. To tackle these issues, data-driven approaches have been recently developed as an alternative to PF approximation. Data-driven PF linearization [7], [8] is used to select the operating point better. Similarly, machine learning (ML) models trained from realistic PF scenarios can improve the accuracy of PWL-PF approximation, by using the  $K$ -plane regression [9] or neural networks (NNs) [10], [11]. The ReLU-based NNs are used to construct simple yet accurate PWL models by incorporating the PF Jacobian information [10]. Similar ideas have been explored in the constraint learning framework [11], [12] but for constraints other than nonlinear PF. Interestingly, these ReLU-based NNs enable the reformulation of the PWL models into mixed-integer linear programs (MILPs), for which efficient off-the-shelf solvers exist.

Despite their success, existing data-driven approaches using end-to-end ML are still challenged by large-scale system applications especially considering topology optimization. First, the number of NN parameters can quickly scale up with the system size, requiring a training dataset of very high quantity and quality. To address the scalability, physics-informed NNs have been considered in [13], [14] for power system problems, but they have not been specifically developed for the problem of PF approximation. Second, these end-to-end ML approaches focus on PF prediction for a fixed topology and are unable to incorporate topology variables. The latter is of great interest in OTS/ROP-typed optimization tasks in order to increase grid flexibility and resilience.

To this end, our goal is to develop a data-driven approach to obtain linearizable PF models that uniquely build upon the generative structure of PF equations. Our proposed PWL approximation nicely incorporates the physical Ohm's Law and nodal power balance into the NN layer design. Specifically, it predicts the nonlinear sinusoidal terms that are common to all PF variables using a ReLU-based hidden layer, and further maps to all line flows and nodal injections using two linear layers. Using this structural design and joint training across layers, our generative NN (GenNN) can ensure excellent consistency among all the predicted PF variables. Interestingly, the last GenNN layer from line flows to nodal injections can naturally allow for a flexible topology by using binary decision variables to indicate line status. To reduce the GenNN model complexity, we propose to sparsify the weight parameters

This work has been supported by NSF Grants 2130706 and 2150571.

The authors are with the Chandra Family Department of Electrical & Computer Engineering, The University of Texas at Austin, Austin, TX, 78712, USA; Emails: {jacobcho, haozhu}@utexas.edu.

based on partitioning the large system into multiple areas, each of a fixed small size. This way, the total number of weight parameters grows only linearly with the system size, and our spectral clustering-based partitioning also allows the GenNN to exploit the weak couplings within a large interconnection. Thanks to our sparse GenNN design, we can attain highly accurate PWL-PF models for power systems with thousands of nodes and use them to efficiently solve the AC-OTS/ROP as MILPs. We have validated improvements of our GenNN models in PF consistency and accuracy over existing end-to-end, direct NN approaches, using the IEEE 118-bus test case [15] and the 6716-bus synthetic Texas grid case [16]. In addition, the resultant PWL models can produce AC-OTS/ROP solutions with excellent optimality/feasibility performances at only the computation complexity of the DC counterparts. In a nutshell, our main contributions are three-fold:

- 1) We develop a data-driven GenNN model that can provide accurate PWL approximation of AC-PF while maintaining the consistency among different PF variables;
- 2) We design the sparse GenNN to reduce the model complexity by exploiting the weak PF coupling among areas, that can easily scale up to large interconnections.
- 3) Our GenNN model includes a varying grid topology as decision variables, enabling an MILP-based reformulation of a variety of grid topology optimization tasks.

The rest of the paper is organized as follows. Section II presents the AC-PF modeling. Section III discusses the GenNN model and its sparsification using area partitioning. In Section IV, we develop the steps for MILP reformulation of grid optimization by simplifying the equivalent constraints. Section V presents the numerical results to demonstrate the performance improvements attained by our proposed schemes, and Section VI wraps up the paper.

## II. AC POWER FLOW MODELING

We first present the nonlinear AC-power flow (PF) modeling to be used by our proposed data-driven model later on. Consider a transmission system consisting of  $N$  buses collected in the set  $\mathcal{N} := \{1, \dots, N\}$  and  $L$  branches in  $\mathcal{L} := \{(i, j)\} \subset \mathcal{N} \times \mathcal{N}$ . For each bus  $i \in \mathcal{N}$ , let  $V_i \angle \theta_i$  denote the complex nodal voltage phasor, and  $\{P_i, Q_i\}$  denote the active and reactive power injections, respectively. For each branch  $(i, j) \in \mathcal{L}$ , let  $\theta_{ij} := \theta_i - \theta_j$  denote the angle difference between buses  $i$  and  $j$ , with  $\{P_{ij}, Q_{ij}\}$  the active and reactive power flows from bus  $i$  to  $j$ . In addition, the branch's series and shunt admittance values are respectively denoted by  $y_{ij} = g_{ij} + jb_{ij}$  and  $y_{ij}^{\text{sh}} = g_{ij}^{\text{sh}} + jb_{ij}^{\text{sh}}$ .

The power flows of branch  $(i, j)$  depend on  $\{V_i, V_j, \theta_{ij}\}$ , and in the case of a transformer, its tap ratio  $a_{ij}$ , as given by

$$P_{ij} = V_i^2 \left( \frac{g_{ij}}{a_{ij}^2} + g_i^{\text{sh}} \right) - \frac{V_i V_j}{a_{ij}} (g_{ij} \cos \theta_{ij} + b_{ij} \sin \theta_{ij}), \quad (1a)$$

$$Q_{ij} = -V_i^2 \left( \frac{b_{ij}}{a_{ij}^2} + b_i^{\text{sh}} \right) - \frac{V_i V_j}{a_{ij}} (g_{ij} \sin \theta_{ij} - b_{ij} \cos \theta_{ij}). \quad (1b)$$

The following nonlinear terms can capture the coupling between active and reactive power flows in (1):

$$\gamma_i := V_i^2, \quad \rho_{ij} := V_i V_j \cos \theta_{ij}, \quad \text{and} \quad \pi_{ij} := V_i V_j \sin \theta_{ij}. \quad (2)$$

Note that both power flows are linear combinations of these nonlinear terms, based on the branch parameters  $\{y_{ij}, y_{ij}^{\text{sh}}, a_{ij}\}$ . For transmission lines,  $a_{ij}$  is simply set to 1. For transformers, the tap ratio  $a_{ij}$  is typically within the range of  $[0.9, 1.1]$  and only affects the primary-to-secondary direction. Thus, for the secondary-to-primary direction, one can also use  $a_{ij} = 1$  in (1). While this work assumes  $a_{ij}$  is given, it is possible to include controllable tap ratios as optimization's decision variables; see e.g., [17].

The power injections to bus  $i$  can be formed by  $\{P_{ij}, Q_{ij}\}$  and the corresponding branch status denoted by  $\epsilon_{ij} \in \{0, 1\}$  (0/1: off/on), as given by

$$P_i = \sum_{(i,j) \in \mathcal{L}} \epsilon_{ij} P_{ij}, \quad (3a)$$

$$Q_i = \sum_{(i,j) \in \mathcal{L}} \epsilon_{ij} Q_{ij}. \quad (3b)$$

The binary variables  $\{\epsilon_{ij}\}$  will be important for formulating grid optimization tasks with varying topology, as detailed later on. With no topology changes, they can be fixed at  $\epsilon_{ij} = 1$ .

One can view the above AC-PF model as a sequential transformation from the angles and voltages to i) the nonlinear terms, ii) line power flows, and iii) bus injections. To represent this transformation, let us concatenate all the power flows and injections in  $\mathbf{z}^{pf} \in \mathbb{R}^{4L}$  and  $\mathbf{z}^{inj} \in \mathbb{R}^{2N}$ . In addition, let  $\boldsymbol{\gamma} \in \mathbb{R}^N$ ,  $\boldsymbol{\rho} \in \mathbb{R}^L$ , and  $\boldsymbol{\pi} \in \mathbb{R}^L$  denote the vector-forms of the three types of nonlinear terms. This way, we have

$$\mathbf{z}^{pf} = \mathbf{W}^\gamma \boldsymbol{\gamma} + \mathbf{W}^\rho \boldsymbol{\rho} + \mathbf{W}^\pi \boldsymbol{\pi}, \quad (4a)$$

$$\mathbf{z}^{inj} = \mathbf{W}^\psi \mathbf{z}^{pf} \quad (4b)$$

where the weight matrices  $\{\mathbf{W}^\gamma, \mathbf{W}^\rho, \mathbf{W}^\pi, \mathbf{W}^\psi\}$  are of appropriate dimensions using the given branch parameters and branch status variables in (1) and (3). Clearly, the introduction of nonlinear terms makes the rest of transformations in (4a)-(4b) purely linear. Thus, our proposed NN model will represent (4) as linear layers and use the nonlinear layers only to form  $\{\boldsymbol{\gamma}, \boldsymbol{\rho}, \boldsymbol{\pi}\}$  in (2).

We also discuss the standard PF linearization around a given operating point, which will be used for the design of PWL approximation. We consider the first-order approximation method, while there also exist other linearization techniques such as the fixed-point method [18]. Consider the vector  $\mathbf{x}$  consisting of all input variables in  $\{V_i\}_{i \in \mathcal{N}}$  and  $\{\theta_{ij}\}_{(i,j) \in \mathcal{L}}$ , and a given operating point denoted by  $\check{\mathbf{x}}$  along with  $\{\check{V}_i, \check{\theta}_{ij}\}$ . To linearize  $\boldsymbol{\gamma}$ , we can use  $\hat{\gamma}_i = 2V_i - \check{V}_i$ ,  $\forall i \in \mathcal{N}$ , by using the fixed  $\check{V}$ . As shown in [5], for power systems with well-regulated bus voltages this linearized approximation vector  $\hat{\boldsymbol{\gamma}}$  can attain very high accuracy. As for the two nonlinear terms in  $[\boldsymbol{\rho}; \boldsymbol{\pi}] = \mathbf{f}(\mathbf{x}) \in \mathbb{R}^{2L}$ , where  $\mathbf{f}(\cdot)$  represents the nonlinear mapping described in (2). For given  $\check{\mathbf{x}}$ , the first-order approximation becomes

$$\hat{\boldsymbol{\gamma}} = 2\mathbf{V} - \check{\mathbf{V}}, \quad \text{and} \quad [\hat{\boldsymbol{\rho}}; \hat{\boldsymbol{\pi}}] = \mathbf{f}(\check{\mathbf{x}}) + \check{\mathbf{J}}\check{\mathbf{x}} \quad (5)$$

where  $\check{\mathbf{J}}$  denotes the Jacobian matrix of  $\mathbf{f}(\cdot)$  evaluated at  $\check{\mathbf{x}}$ , while  $\check{\mathbf{x}} := \mathbf{x} - \check{\mathbf{x}}$  stands for the deviation from  $\check{\mathbf{x}}$ . Due to the sinusoidal relations, the linearization in  $[\hat{\boldsymbol{\rho}}; \hat{\boldsymbol{\pi}}]$  could suffer from high inaccuracy issue, especially with a large angle difference. Therefore, the ensuing section will build the PWL model to improve the approximation of  $[\boldsymbol{\rho}; \boldsymbol{\pi}]$ .

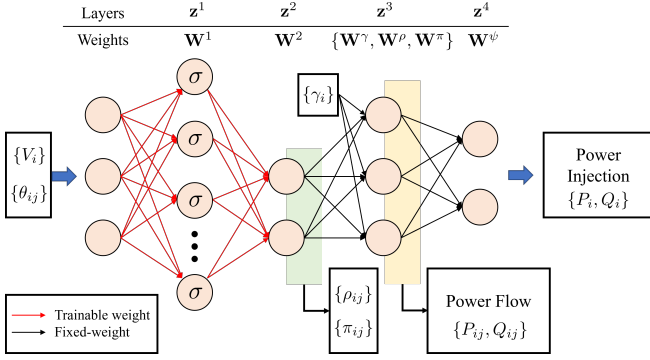


Fig. 1: The proposed GenNN model predicts the nonlinear terms in the second layer using trainable weights; it further generates power variables in the third/fourth layers to match the PF equations.

### III. GENNN FOR PWL APPROXIMATION

We develop the PWL model of PF equations by using a generative neural network (GenNN) structure. Fig. 1 illustrates the overall architecture of our proposed design. The first two layers predict the nonlinear terms  $[\rho; \pi]$ , and the following two *linear* layers generate the power flows and injections. The ReLU activation  $\sigma(\cdot)$  in the first (hidden) layer can lead to a PWL model for  $[\hat{\rho}; \hat{\pi}]$  while adjusting the GenNN parameters therein can improve the accuracy of the approximation. The full structure of the GenNN becomes

$$\mathbf{z}^1 = \sigma(\mathbf{W}^1 \tilde{\mathbf{x}} + \mathbf{b}), \quad (6a)$$

$$\mathbf{z}^2 = \mathbf{f}(\tilde{\mathbf{x}}) + (\tilde{\mathbf{J}} \tilde{\mathbf{x}} + \mathbf{W}^2 \mathbf{z}^1), \quad (6b)$$

$$\mathbf{z}^3 = \mathbf{W}^\gamma \hat{\boldsymbol{\gamma}} + [\mathbf{W}^\rho; \mathbf{W}^\pi] \mathbf{z}^2, \quad (6c)$$

$$\mathbf{z}^4 = \mathbf{W}^\psi \mathbf{z}^3. \quad (6d)$$

Note that the second layer has utilized the linear approximation in (5) by using the given operating point  $\tilde{\mathbf{x}}$ . Moreover, the third layer of our GenNN needs to use the squared voltage, for which the linearized  $\hat{\boldsymbol{\gamma}}$  in (5) can be adopted thanks to its high accuracy. To obtain the trainable GenNN parameters  $\{\mathbf{W}^1, \mathbf{W}^2, \mathbf{b}\}$ , the Euclidean distance can be employed to construct the loss function. Based on the input samples, we can calculate the errors between the actual  $\mathbf{f}(\mathbf{x}) = [\rho; \pi]$  and the vector  $\mathbf{z}^2$  generated by the GenNN. In addition, the loss function can include the errors between the actual  $[\mathbf{z}^{pf}; \mathbf{z}^{inj}]$  and the GenNN outputs  $[\mathbf{z}^3; \mathbf{z}^4]$  to ensure consistency among all PF variables, given by

$$\begin{aligned} \mathcal{L}(\mathbf{W}^1, \mathbf{W}^2, \mathbf{b}) = & \|\mathbf{f}(\mathbf{x}) - \mathbf{z}^2\|_2^2 \\ & + \lambda \|\llbracket [\mathbf{z}^{pf}; \mathbf{z}^{inj}] - [\mathbf{z}^3; \mathbf{z}^4] \rrbracket\|_2^2 \end{aligned} \quad (7)$$

To balance the two error terms, we set  $\lambda > 0$  as a regularization hyperparameter. The choice of  $\lambda$  can affect the prediction of the PF variables, as a larger  $\lambda$  leads to higher consistency and accuracy in the last two layers. The proposed GenNN design along with the weighted loss function can ensure a consistent match of the PF equations, which will be demonstrated by extensive numerical tests.

By using the ReLU activation in (6a), the first two layers extend the linearized model in (5) to a PWL function. Note that

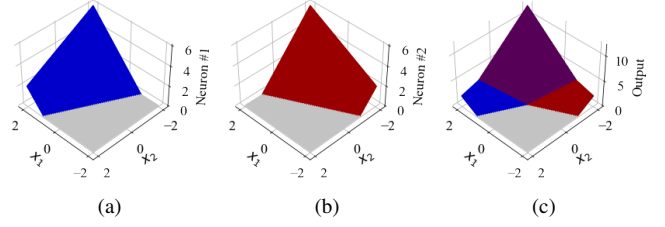


Fig. 2: Each ReLU-based hidden neuron (a)-(b) produces a PWL function with two linear regions. The sum of the two neurons (c) becomes another PWL function with four linear regions due to the combination of two neurons' activation status.

each hidden neuron  $z_k^1$  in (6a) essentially uses the activation status to divide the total input space into two different linear regions, forming a PWL relation. To this end, consider a  $2 \times 1$  input vector  $\mathbf{x} = [x_1; x_2]$  with two hidden neurons. As illustrated in Figs. 2(a)-(b), each of the two hidden neurons produces a PWL relation with two linear regions. The linear combination of these two outputs further divides into multiple linear regions, as shown by Fig. 2(c), consisting of four linear regions per the combination of the two ReLU functions' activation status. By using multiple hidden neurons in (6a), our proposed GenNN can express a complex PWL model.

Clearly, the expressiveness of the GenNN depends on the total number of linear regions produced by the ReLU-based hidden layer, making it important to select the number of hidden neurons. As the number of linear regions scales with the combination of all ReLUs' activation, it can go as high as  $2^K$  for a given  $K$  hidden neurons. Thus, a large enough  $K$  has to be used to ensure the resultant PWL model can achieve an accurate approximation. Nonetheless, there is a trade-off between the accuracy and the model complexity by varying  $K$ , as the total number of GenNN parameters to be trained also increases with  $K$ . In addition, a high model complexity may lead to a lack of generalizability, namely a loss of accuracy with testing samples that have not been used for training. This is related to the *curse of dimensionality*, a well-known paradox in statistical learning [19]. Hence, selecting an appropriate  $K$  would be critical to ensure a good balance between expressiveness and generalizability. We provide some insights on this selection here.

**Remark 1.** (Selecting the number of hidden neurons.) As the dimensions of the GenNN's inputs/outputs depend on  $N$  and  $L$ , the numbers of buses/lines, we expect the number of hidden neurons  $K$  should scale with them to attain sufficient accuracy. To choose  $K$ , we have tested the approximation performance of the first two GenNN layers using the IEEE 14-bus system with either 20 or 15 lines, with the latter having 5 lines deleted from the original test case. Fig. 3 plots the average approximation errors versus  $K$  for both systems, which suggests a good choice for  $L = 15$  would be  $K = 14$  and for  $L = 20$  would be  $K = 19$ . We have further performed similar tests in larger systems, and our experimental experiences confirm that  $K \approx (2N/3 + L/3)$  would lead to a good approximation accuracy.

Thus, the number of hidden neurons  $K$  needed for our

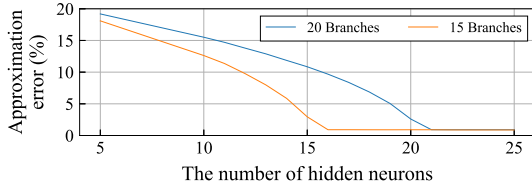


Fig. 3: Error performance versus the number of hidden neurons for the IEEE 14-bus system with either 20 or 15 branches.

GenNN grows with the system size. Assuming the number of lines  $L \sim \mathcal{O}(N)$  as in typical power systems [20], this choice of  $K$  is also in  $\mathcal{O}(N)$ . With fully-connected weight matrices  $\{\mathbf{W}^1, \mathbf{W}^2\}$ , the total number of parameters is  $\mathcal{O}((N+L)K)$  which becomes  $\mathcal{O}(N^2)$ . This quadratic growth rate inspires us to consider sparsifying the weight matrices by partitioning the system into fixed-sized areas.

#### A. Sparsifying GenNN using Area Partitioning

To improve the GenNN’s scalability, we will partition the power system into multiple areas, all of which are kept at a certain fixed size. This area partitioning would allow to scale the number of parameters according to the area’s size without growing with the overall system size. In fact, having fully-connected weight matrices  $\{\mathbf{W}^1, \mathbf{W}^2\}$  does not match with the PF equations in (1), where line flows  $\{P_{ij}, Q_{ij}\}$  only depend on the voltages/angles at its own end buses. Hence, building the GenNNs for each area could also improve the match with PF equations by eliminating the dependency on the inputs from other areas. Consider the example of a small 4-bus system in Fig. 4, which consists of two areas with a line connecting different areas (known as a tie-line). Within the top area formed by buses 1 and 2, the line flows  $\{P_{12}, Q_{12}\}$  only depend on the inputs within this area, but not on the bottom area. If we do not consider the tie-line, then a GenNN can be separately formed for each of the two areas, as shown by the top and bottom parts of the GenNN layers in Fig. 4. Therefore, area partitioning can effectively sparsify the GenNN weight matrices  $\{\mathbf{W}^1, \mathbf{W}^2\}$  into block-diagonal submatrices, each of which scales with the fixed area size. For a system of  $N$  buses with each area of  $N' = 25$  buses, the number of weight parameters becomes  $\mathcal{O}((N')^2(N/N')) \sim \mathcal{O}(N \cdot N')$ , which is linear in  $N$  instead of quadratic. This is a significant reduction for large systems.

Nonetheless, the presence of tie-lines requires connecting the decoupled GenNNs among two neighboring areas. This tie-line coupling can be conveniently incorporated by expanding the area’s inputs with the end bus from the neighboring area. As shown in Fig. 4, the tie-line between buses 2 and 3 uses the inputs from both of the two areas. Thus, to predict the line flows  $\{P_{23}, Q_{23}\}$ , the top part of GenNN can be modified by adding the inputs  $\{V_3, \theta_{23}\}$ . This modification could create a few additional entries to  $\{\mathbf{W}^1, \mathbf{W}^2\}$ , but the weight matrices are in an almost block-diagonal form with very high sparse level. For small systems, these sparse  $\{\mathbf{W}^1, \mathbf{W}^2\}$  can be similarly trained as the case of full matrices earlier, by keeping the zero entries during the training process. When the system

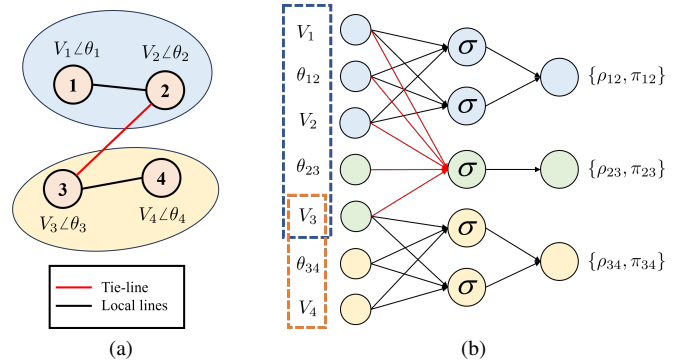


Fig. 4: (a) A 4-bus system with two areas and a tie-line; and (b) its sparse GenNN. Two individual GenNNs (blue and yellow) are separately formed for the two areas, while the tie-line is incorporated into the top GenNN by introducing more input variables ( $\theta_{23}$  and  $V_3$ ).

size increases, the area-based submatrices can be separately trained using the inputs/outputs within each of the areas including the tie-lines, as discussed later in Remark 2. Either way, the total number of trainable parameters in the GenNN can be significantly reduced thanks to the area partitioning-based sparsification.

Since the level of coupling in GenNN depends on the tie-lines, the area partitioning should be designed to reduce the total number, or generally speaking, the *electrical connectivity*, of the tie-lines. To this end, we propose to perform the *spectral clustering* on the underlying graph of the power network, which can effectively reduce the inter-area connectivity while producing clusters of high intra-area connectivity [21]. Specifically, we assign a weight parameter for each branch  $(i, j)$  using its series impedance, as given by  $\lambda_{ij} := \frac{1}{|z_{ij}|}$  with  $z_{ij} = 1/y_{ij}$ . This weight choice of  $\lambda_{ij}$  follows from the so-termed *electrical distance* between two neighboring buses [22], as a very small line impedance implies that the two end buses are electrically very close. To minimize the total electrical distances, or weights, of the tie-lines, the spectral clustering works by performing the spectral analysis of the weighted graph Laplacian matrix  $\mathbf{\Lambda} \in \mathbb{R}^{N \times N}$ , defined by

$$\mathbf{\Lambda}_{ij} = \begin{cases} \sum_{j=1}^n \lambda_{ij}, & \text{if } i = j, \\ -\lambda_{ij}, & \text{if } (i, j) \in \mathcal{L}, \\ 0, & \text{otherwise.} \end{cases}$$

Consider the eigen-decomposition of the symmetric matrix  $\mathbf{\Lambda} = \mathbf{R}\mathbf{S}\mathbf{R}^T$  with the diagonal matrix  $\mathbf{S}$  having the eigenvalues  $s_1 \leq s_2 \leq \dots \leq s_N$  and  $\mathbf{R} = [\mathbf{r}_1; \mathbf{r}_2; \dots; \mathbf{r}_N]$  containing the eigenvectors as the columns. Since  $\mathbf{\Lambda}$  is a graph Laplacian matrix, it is known that the smallest eigenvalue  $s_1 = 0$  with  $\mathbf{r}_1$  related to the all-one vector [23]. In this sense, this eigenvector “equally” represents all the nodes throughout the network. Generally speaking, the eigenvectors associated with smaller eigenvalues tend to capture more the global connectivity among the nodes while those with larger eigenvalues tend to represent the local connectivity. For example, if the second smallest eigenvalue  $s_2 = 0$ , then the graph has to consist of two disconnected areas. Thus, if we select the  $C$ -smallest eigenvalues after  $s_1$ , namely  $s_2, \dots, s_{C+1}$ , then the corresponding eigenvectors in  $[\mathbf{r}_2; \dots; \mathbf{r}_{C+1}] \in \mathbb{R}^{N \times C}$  can be

used to form the  $C$  features for the  $N$  nodes. This feature matrix allows to partition the nodes into up to  $2^C$  areas using e.g., the  $k$ -means clustering. It is also possible to use the unweighted graph Laplacian with  $\lambda_{ij} = 1$  (or other weight designs) for every branch, which could lead to an area partition with a minimal number of tie-lines. We have tested both types of Laplacian matrices for spectral clustering, and they yield similar results. The weighted Laplacian using the electrical distance could reduce the PF couplings among the areas, and thus is the preferred metric for our spectral clustering approach. Upon training the sparse GenNN, we can produce a concise yet effective PWL approximation for the system-wide PF model.

**Remark 2.** (*Training for large-scale systems*) When the system size is large with e.g.  $N \geq 1000$ , it could become very computationally demanding to allocate all the weight parameters into the computer memory for training. One solution to improve the memory efficiency is to separately build the GenNN for each area, using the inputs/outputs within the area. Note that every tie-line could be assigned to one of the connected areas, which completely eliminates the PF coupling. Basically, for the network in Fig. 4, we could separately train the two parts of GenNN, as marked by the dashed boxes. While this simple decoupled training could lose some approximation accuracy comparing to a joint training among all weight parameters, our numerical experiments have suggested the former still attains a very high approximation performance at a significant reduction of memory needs.

#### IV. GENNN FOR MILP-BASED GRID OPTIMIZATION

We formulate our GenNN-based PWL-PF model into a mixed-integer linear (MIL) form, which will be utilized by a variety of grid optimization problems later on. Recall that for the GenNN model (6), the only nonlinearity lies in the first layer in (6a). Thus, it suffices to consider the reformulation of the ReLU functions therein only. To this end, we have

$$\mathbf{z}^1 = \sigma(\mathbf{W}^1 \tilde{\mathbf{x}} + \mathbf{b}) = (\mathbf{W}^1 \tilde{\mathbf{x}} + \mathbf{b}) \odot \beta \quad (8)$$

where  $\beta$  is an auxiliary binary vector indicating the ReLU activation status, while  $\odot$  denotes the entry-wise vector multiplication. This representation allows us to adopt the well-known *big-M tightening method* for an equivalent linear reformulation [24]. As detailed soon, it is possible to the upper/lower bounds of the continuous vector  $(\mathbf{W}^1 \tilde{\mathbf{x}} + \mathbf{b})$  to express (8) using four linear inequalities. Note that the complexity of the resultant MIL formulation can be significantly reduced by: i) selecting very tight upper/lower bounds; and ii) eliminating the subset of inequalities that are inactive. We will discuss how to design these two very important aspects specifically for formulating the NN-based relation in (8).

The tightness of the upper/lower bounds on the continuous vector crucially affects the computation complexity of the resultant optimization [25]. For example, these bounds could be determined based on the range of the input vector, namely  $\tilde{\mathbf{x}} \in [\underline{\mathbf{x}}, \bar{\mathbf{x}}]$ . The latter is easy to obtain for our grid optimization problems, by using the system operating limits on voltage/angle variables as detailed later. Using the

range  $[\underline{\mathbf{x}}, \bar{\mathbf{x}}]$ , one could bound  $(\mathbf{W}^1 \tilde{\mathbf{x}} + \mathbf{b})$  by casting some optimization problems; see e.g., [10]. Nonetheless, solving the resultant optimization problems inevitably incurs additional computation time. Instead of using this optimization step, recent work [26] has developed a direct approach for this bounding specifically for the linear form of  $(\mathbf{W}^1 \tilde{\mathbf{x}} + \mathbf{b})$ . Let us form two matrices  $\{\mathbf{L}, \mathbf{U}\} \in \mathbb{R}^{N \times K}$  according to the sign of the entries in  $\mathbf{W}^1$ , as given by

$$\{L_{nk}, U_{nk}\} = \begin{cases} \{\underline{x}_n, \bar{x}_n\} & \text{if } W_{kn}^1 \geq 0 \\ \{\bar{x}_n, \underline{x}_n\} & \text{if } W_{kn}^1 < 0 \end{cases}. \quad (9)$$

Using these two matrices, we can express the  $k$ -th entry in (8), namely  $z_k^1$ , via four linear inequalities:

$$0 \leq z_k^1 \leq (\mathbf{W}_{k:}^1 \mathbf{U}_{:k} + b_k) \beta_k, \quad (10a)$$

$$\mathbf{W}_{k:}^1 \tilde{\mathbf{x}} + b_k \leq z_k^1 \leq \mathbf{W}_{k:}^1 (\tilde{\mathbf{x}} - \mathbf{L}_{:k} (1 - \beta_k)) + b_k \beta_k, \quad (10b)$$

where  $\mathbf{W}_{k:}^1$  denotes the  $k$ -th row of matrix  $\mathbf{W}^1$ . Basically, if the term  $\mathbf{W}_{k:}^1 \tilde{\mathbf{x}} + b_k > 0$ , then the inequality  $z_k \geq \mathbf{W}_{k:}^1 \tilde{\mathbf{x}} + b_k$  in (10b) would force  $\beta_k = 1$ , and thus  $z_k^1 = \mathbf{W}_{k:}^1 \tilde{\mathbf{x}} + b_k$ , to hold in (10a). Otherwise, if  $\mathbf{W}_{k:}^1 \tilde{\mathbf{x}} + b_k < 0$ , then the inequality  $z_k \geq 0$  in (10a) would force  $\beta_k = 0$  to hold in (10b). Substituting  $\beta_k = 0$  into (10a) leads to  $z_k^1 = 0$ . It is shown in [26] that these four linear inequalities based on the range of  $\tilde{\mathbf{x}}$  can attain a much tighter big-M reformulation over traditional bounding approaches. This can greatly improve the solution efficiency of the resultant MILP; see e.g., [26] for more discussions.

In addition to facilitating the bounding, the range of  $\tilde{\mathbf{x}}$  can be used for directly determining certain  $\beta_k$ 's, and accordingly the activation status of some inequalities in (10). Those inactive inequalities can be eliminated in the resulting MILP, further improving the computation efficiency. Note that if the ReLU activation status for the  $k$ -th neuron  $z_k^1$  remains unchanged for the entire range of  $\tilde{\mathbf{x}}$ , then we can directly set the value of  $\beta_k$  to be either 0 or 1. Specifically, if  $\mathbf{W}_{k:}^1 \mathbf{U}_{:k} + b_k < 0$ , then  $\beta_k = 0$  and thus  $z_k^1 = 0$  have to hold for any  $\tilde{\mathbf{x}}$  in order to satisfy (10a). This way, the inequalities in (10b) are no longer active. Similarly, if  $\mathbf{W}_{k:}^1 \mathbf{L}_{:k} + b_k \geq 0$ , then  $\beta_k = 1$  and thus  $z_k^1 = \mathbf{W}_{k:}^1 \tilde{\mathbf{x}} + b_k$  have to hold for any  $\tilde{\mathbf{x}}$  to satisfy (10b), making the inequalities in (10a) inactive. Hence, we define two subsets of the neurons  $k \in \mathcal{K} := \{1, \dots, K\}$ :

$$\mathcal{K}_0 = \left\{ k \in \mathcal{K} \mid \mathbf{W}_{k:}^1 \mathbf{U}_{:k} + b_k < 0 \right\}, \quad (11a)$$

$$\mathcal{K}_1 = \left\{ k \in \mathcal{K} \mid \mathbf{W}_{k:}^1 \mathbf{L}_{:k} + b_k \geq 0 \right\}. \quad (11b)$$

For any neuron  $k \in \mathcal{K}_0$ , it suffices to fix  $\beta_k = 0$  and apply only (10a); and similarly for any  $k \in \mathcal{K}_1$ , it suffices to fix  $\beta_k = 1$  and apply only (10b). This way, we can reduce the total number of linear inequalities while maintaining the equivalence of the formulation. Based on our empirical experiences, this step could reduce the number of binary variables for our GenNN representation by around 5%.

These two steps allow us to reformulate the GenNN-based PF model in (6a)-(6c) into:

$$\mathbf{W}_{k:}^1 \tilde{\mathbf{x}} + b_k \leq z_k^1 \leq \mathbf{W}_{k:}^1 (\tilde{\mathbf{x}} - \mathbf{L}_{:k} (1 - \beta_k)) + b_k \beta_k, \quad \forall k \in \mathcal{K} - \mathcal{K}_0 \quad (12a)$$

$$0 \leq z_k^1 \leq (\mathbf{W}_{k:}^1 \mathbf{U}_{:k} + b_k) \beta_k, \quad \forall k \in \mathcal{K} - \mathcal{K}_1 \quad (12b)$$

$$\beta_k = \begin{cases} 1, & k \in \mathcal{K}_1 \\ 0, & k \in \mathcal{K}_0 \end{cases} \quad (12c)$$

$$[\hat{\rho}; \hat{\pi}] = [\underline{\rho}; \bar{\pi}] + \tilde{\mathbf{J}}\tilde{\mathbf{x}} + \mathbf{W}^2\mathbf{z}^1 \quad (12d)$$

$$\hat{\gamma} = 2\mathbf{V} - \tilde{\mathbf{V}} \quad (12e)$$

$$P_{ij} = \hat{\gamma}_i \left( \frac{g_{ij}}{a_{ij}^2} + g_i^{\text{sh}} \right) - \frac{g_{ij}}{a_{ij}} \hat{\rho}_{ij} - \frac{b_{ij}}{a_{ij}} \hat{\pi}_{ij}, \quad \forall (i, j) \in \mathcal{L}, \quad (12f)$$

$$Q_{ij} = -\hat{\gamma}_i \left( \frac{b_{ij}}{a_{ij}^2} + b_i^{\text{sh}} \right) + \frac{b_{ij}}{a_{ij}} \hat{\rho}_{ij} - \frac{g_{ij}}{a_{ij}} \hat{\pi}_{ij}, \quad \forall (i, j) \in \mathcal{L}. \quad (12g)$$

Basically, we express the first layer (6a) into the linear inequalities in (12a)-(12c), while the following two linear layers remain unchanged. Recall that the squared voltage  $\gamma$  in (12e) adopts a simple first-order approximation. This MIL representation of PF can be incorporated into various grid optimization problems to attain an MILP reformulation. We first consider the clairvoyant AC-OPF here, which will be generalized to problems with flexible topology soon. Given the cost function  $c_i(\cdot)$  in providing nodal flexibility at bus  $i$ , the AC-OPF seeks to minimize the total cost while satisfying the operation limits, as given by

$$\min \sum_{i=1}^N c_i(P_i) \quad (13a)$$

$$\text{s.t. } \underline{V}_i \leq V_i \leq \bar{V}_i, \quad \underline{\theta}_{ij} \leq \theta_{ij} \leq \bar{\theta}_{ij}, \quad \beta_k \in \{0, 1\}, \quad (13b)$$

$$\underline{P}_i \leq P_i \leq \bar{P}_i, \quad \underline{Q}_i \leq Q_i \leq \bar{Q}_i, \quad (13c)$$

$$\underline{P}_{ij} \leq P_{ij} \leq \bar{P}_{ij}, \quad \underline{Q}_{ij} \leq Q_{ij} \leq \bar{Q}_{ij}, \quad (13d)$$

$$(3) \text{ and } (12). \quad (13e)$$

Note that this generic AC-OPF formulation uses  $P_i$  and  $Q_i$  to represent bus  $i$ 's total injection flexibility from both generation and demand. The constraints in (13b) represent the safety limits for the voltage/angle decision variables, and set up the binary activation variable. Moreover, the power limits in (13c) can account for the presence of non-controllable resources such as the fixed demand, in addition to the resource limits. Furthermore, the line flow constraints in (13d) are used to mitigate line overloading. While for simplicity only active/reactive flows are considered here, it is also common to include a constraint on apparent power flow limit. This could be possibly done by either extending our GenNN model to predict apparent line flows or using a quadratic inequality like  $P_{ij}^2 + Q_{ij}^2 \leq (\bar{S}_{ij})^2$ . Finally, the inclusion of (3) ensures the nodal power balance with given line connectivity in  $\epsilon_{ij}$ 's. Clearly, the problem (13) is an MILP thanks to the linear reformulation for the PWL-PF as in (12). By allowing the line status  $\{\epsilon_{ij}\}$  in (3) to be decision variables, we can extend this AC-OPF formulation to general grid optimization problems with flexible topology. We present two such problems to demonstrate the importance of our topology-aware GenNN design for power flow representation.

### A. Optimal Transmission Switching

The AC optimal transmission switching (OTS) problem aims to determine the line switching in addition to the nodal flexibility in AC-OPF [1]. Hence, the OTS problem is capable of increasing the grid operational flexibility. Nonetheless, solving OTS, especially the one based on AC power flow, is

challenged by the presence of integer decision variables used for selecting the line status. Our proposed PWL-PF model can facilitate the reformulation of AC-OTS into MILP. To this end, let us denote  $\hat{P}_{ij} := \epsilon_{ij} P_{ij}$  and  $\hat{Q}_{ij} := \epsilon_{ij} Q_{ij}$  in (3), where the line status  $\epsilon_{ij}$  becomes a binary decision variable in OTS. To deal with these multiplication terms, we can similarly apply the big-M tightening method for an MIL representation by adding additional constraints to the AC-OPF (13), as below:

$$\min \sum_{i=1}^N c_i(P_i) \quad (14a)$$

$$\text{s.t. } (13b) - (13e), \quad \epsilon_{ij} \in \{0, 1\} \quad (14b)$$

$$\underline{P}_{ij} \epsilon_{ij} \leq \hat{P}_{ij} \leq \bar{P}_{ij} \epsilon_{ij}, \quad (14c)$$

$$\underline{Q}_{ij} \epsilon_{ij} \leq \hat{Q}_{ij} \leq \bar{Q}_{ij} \epsilon_{ij}, \quad (14d)$$

$$P_{ij} + \bar{P}_{ij}(\epsilon_{ij} - 1) \leq \hat{P}_{ij} \leq P_{ij} + \underline{P}_{ij}(\epsilon_{ij} - 1), \quad (14e)$$

$$Q_{ij} + \bar{Q}_{ij}(\epsilon_{ij} - 1) \leq \hat{Q}_{ij} \leq Q_{ij} + \underline{Q}_{ij}(\epsilon_{ij} - 1). \quad (14f)$$

$$\sum_{(i,j) \in \mathcal{L}} \epsilon_{ij} \geq L - \alpha \quad (14g)$$

where the last constraint (14g) sets a total switching budget of no more than  $\alpha$  lines. The constraints (14c)-(14f) are the linear formulation for  $\hat{P}_{ij}$  and  $\hat{Q}_{ij}$ , by using their respective bounds per the big-M method. By reformulating the PWL-PF and line switching relations, we cast the AC-OTS as an MILP, for which efficient solvers will be used as shown by the numerical tests soon.

### B. Restoration Ordering Problem

We consider the power system restoration ordering problem (ROP) [2], which extends the static OPF problem to a multi-period setting. The ROP aims to optimize the restoration order of the damaged transmission lines to maximize the energy served to customers while maintaining system stability. Similar to the OTS problem, the ROP also includes the status of the damaged lines as decision variables, along with the power flow. However, as the instantaneous restoration budget is usually very small due to limited resources, the restoration process has to span over multiple periods and thus the ROP is considered over a time horizon  $\mathcal{T} := \{1, \dots, T\}$ . Given a restoration budget of  $\eta$  lines, the total number of connected lines at time  $t$  is updated by

$$R_t = R_{t-1} + \eta, \quad \forall t \in \mathcal{T}, \quad (15)$$

with  $R_0$  initialized by the post-damage power system. This equality establishes the temporal coupling in the ROP.

The ROP aims to determine the binary line status variables  $\epsilon_{ij,t} \in \{0, 1\}$  per line  $(i, j)$ , and the percentage of load shedding  $x_{i,t} \in [0, 1]$  per bus  $i$ , at every time  $t \in \mathcal{T}$ . With the objective of maximizing the total energy provided to all customers throughout the restoration process, the ROP can be formulated using the PWL-PF model in (12), as

$$\max \sum_{t=1}^T \sum_{i=1}^N x_{i,t} P_{i,t} \quad (16a)$$

$$\text{s.t. } (13b) - (13e), \quad \epsilon_{ij,t} \in \{0, 1\}, \quad x_{i,t} \in [0, 1] \quad (16b)$$

$$\underline{P}_{ij,t} \epsilon_{ij,t} \leq \hat{P}_{ij,t} \leq \bar{P}_{ij,t} \epsilon_{ij,t}, \quad (16c)$$

$$\underline{Q}_{ij,t} \epsilon_{ij,t} \leq \hat{Q}_{ij,t} \leq \bar{Q}_{ij,t} \epsilon_{ij,t}, \quad (16d)$$

$$P_{ij,t} + \bar{P}_{ij,t}(\epsilon_{ij,t} - 1) \leq \hat{P}_{ij,t} \leq P_{ij,t} + \underline{P}_{ij,t}(\epsilon_{ij,t} - 1), \quad (16e)$$

$$Q_{ij,t} + \bar{Q}_{ij,t}(\epsilon_{ij,t} - 1) \leq \hat{Q}_{ij,t} \leq Q_{ij,t} + \underline{Q}_{ij,t}(\epsilon_{ij,t} - 1), \quad (16f)$$

$$\sum_{(i,j) \in \mathcal{L}} \epsilon_{ij,t} \leq R_t, \quad (16g)$$

$$R_t = R_{t-1} + \eta, \quad \epsilon_{ij,t-1} \leq \epsilon_{ij,t}, \quad \epsilon_{ij,T} = 1. \quad (16h)$$

Note that the initial  $\epsilon_{ij,0}$  is given by the post-damage line status, while (16h) sets the final  $\epsilon_{ij,T} = 1$  to ensure a full restoration. Similar to the OTS, the constraints (16c)-(16f) are used to form the actual line flows  $\hat{P}_{ij,t}$  and  $\hat{Q}_{ij,t}$  according to the line status  $\epsilon_{ij,t}$  per time  $t$ . By bounding the total number of connected lines in (16g), the temporal coupling in (16h) ensures that the restoration budget  $\eta$  is met and the restored lines will stay connected throughout the restoration. Thanks to our proposed GenNN-based PWL-PF representation, the ROP can be again cast as an MILP and will be efficiently solved as shown by the ensuing numerical tests.

## V. NUMERICAL STUDIES

We have validated the proposed GenNN modeling approach on the IEEE 118-bus test case [15] and the 6716-bus synthetic grid case [16] for power flow modeling and grid topology optimization tasks. The 6716-bus test case is a synthetic power system developed to represent the geographical coverage of Texas. The GenNN training has been performed in PyTorch with Adam optimizer on a regular laptop with Intel® CPU @ 2.70 GHz, 32 GB RAM, and NVIDIA® RTX 3070 Ti GPU @ 8GB VRAM. We have formulated the OTS and ROP problems through Pyomo [27] and used the Groubi optimization solver [28] to solve the resultant MILPs.

To train the GenNN, we generate 10,000 samples based on the actual PF model, by using the outputs of nonlinear terms  $\{\gamma, \rho, \pi\}$  along with the line flows and nodal injections. For each sample, we generate uniformly distributed voltage magnitudes within the range of [0.94, 1.06] p.u. for the 118-bus case, and of [0.90, 1.10] p.u. for the 6716-bus case, per the voltage limits in each case. Similarly, the voltage angles are randomly varied within  $[-\pi/6, \pi/6]$  radians around the initial operating point. For the reference bus, namely, Bus 69 in the 118-bus system or Bus 111333 in the 6716-bus system, we fix its voltage magnitude and angle at the default values. The NN parameters have been trained via backpropagation using the loss function (7) with  $\lambda = 10$ , with a total of 20e3 epochs and a learning rate of  $2.5e-3$ . Note that the  $\lambda$  value has been chosen through hyperparameter tuning. We have used 90% of the dataset for training and the rest 10% for testing. The NN modeling results and error performance comparisons presented later on are based on the testing data only.

### A. AC Power Flow Modeling

We consider the AC-PF modeling performance to demonstrate the advantages of our GenNN model designs in Fig. 1. We compare it with the baseline NN model that directly predicts all PF variables as in [10] (indicated by DirectNN). Specifically, the DirectNN model is trained using a two-layer NN to predict  $\mathbf{z}^{pf}$  and  $\mathbf{z}^{inj}$  from the input voltage

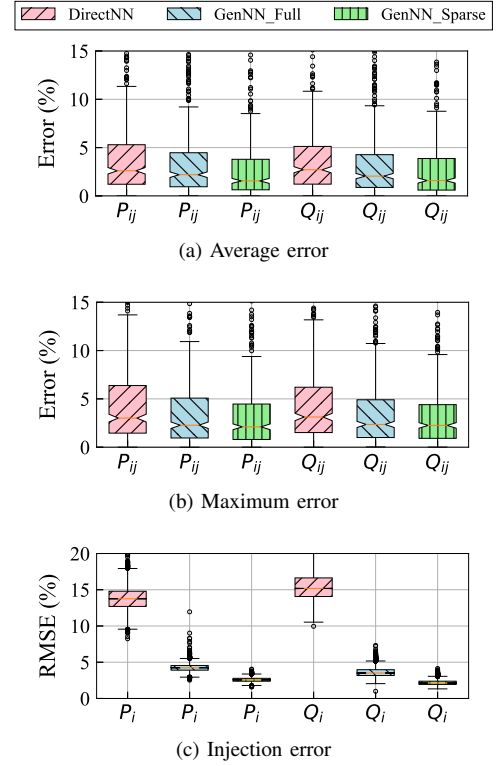


Fig. 5: Comparisons of the (a) average and (b) maximum error in approximating the line power flows and (c) RMSE in predicting the injected power vectors for Direct, GenNN\_Full and GenNN\_Sparse methods using the 118-bus system.

variables  $\mathbf{V}$  and  $\boldsymbol{\theta}$ . We also compare the scalability of the two configurations of our proposed GenNN, the one with fully connected weights (GenNN\_Full) and the one with sparsified weights (GenNN\_Sparse).

First, we present the approximation error performance using the small 118-bus case. All three NN-based models here use a total of  $K = 100$  hidden neurons for the trainable layers, in accordance with Remark 1. To obtain the GenNN\_Sparse model, we partition the system into 5 areas using the  $k$ -means clustering based upon the top 3 eigenvectors of the Laplacian, and the 100 hidden neurons have been uniformly spread across the 5 areas. Fig. 5 shows the error box plots for predicting both the line flows and the power injections. Fig. 5(a) and Fig. 5(b) respectively plot the average and maximum statistics, for the error percentages of both active and reactive line flows as normalized by the line capacity. In addition, Fig. 5(c) shows the root mean square error (RMSE) in predicting the injected power vectors. For the illustration, each box plot indicates the median values as midlines along with the first (Q1) and third (Q3) quartiles as boxes. The horizon bars denote the farthest data points within 1.5 times the interquartile range (Q1-Q3) from the box.

We can observe that compared to DirectNN, the two GenNN models have noticeably reduced the error in approximating both line flows and power injections. This performance improvement of GenNN is especially significant in terms of approximating the injections  $\mathbf{z}^{inj}$  as shown in Fig. 5(c). Since the DirectNN model overlooks the underlying relations between

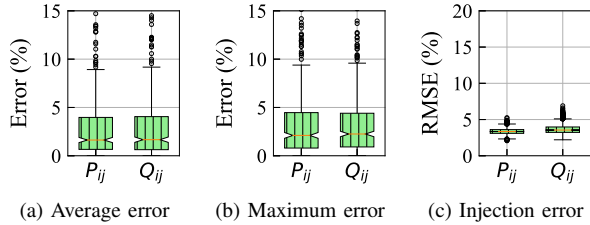


Fig. 6: Comparisons of the (a) average and (b) maximum error in approximating the line power flows and (c) RMSE in predicting the injected power vectors for GenNN\_Sparse using the 6716-bus system.

$\mathbf{z}^{pf}$  and  $\mathbf{z}^{inj}$ , it is prone to produce power flow patterns that are inconsistent with the nodal power balance in (3). In contrast, our GenNN models have been designed to maintain this power flow balance condition thanks to its generative structure between the last two layers in Fig. 1. In addition, Figs. 5(a)-(b) show our GenNN models have also led to some improvements in approximating the line flows  $\mathbf{z}^{pf}$ . This is thanks to the GenNN design by embedding the underlying relations from the nonlinear terms  $\{\gamma, \rho, \pi\}$  to  $\mathbf{z}^{pf}$ . Clearly, the proposed generative structure has shown to be effective for the GenNN-based PWL models to maintain the physical relations among PF variables. Furthermore, the comparisons between the two GenNN models have corroborated the importance of reducing the number of NN parameters, as the GenNN\_Sparse exhibits a higher accuracy than GenNN\_Full. The advantages of having the GenNN\_Sparse design will become even more evident in the large system tests as detailed soon.

To demonstrate the scalability enhancements of the proposed GenNN\_Sparse model, we further test it using the large 6716-bus case. Due to the significant increase in system size, the DirectNN model and even the GenNN\_Full model incur extremely high computational burdens for this large case. The NN training for either of the two models could not be completed within a reasonable time on our computing platform. Therefore, we end up with implementing the GenNN\_Sparse model only here, which can gracefully handle practical systems of a large size as discussed in Remark 2. Specifically, we have partitioned this system into a total of 250 areas by using the top 8 eigenvectors of the Laplacian, leading to approximately 27 nodes in each area on average. This is very close to the area size in the 118-bus case partitioning. A total of  $K = 7500$  hidden neurons has been used for the trainable layers, uniformly spreading across 250 areas. Similar to Fig. 5, we plot the three error statistics in Fig. 6, but only for the GenNN\_Sparse model. Although we cannot compare the performance with the other NN-based models, the level of approximation accuracy by the proposed GenNN\_Sparse is observed to be very similar to that in the 118-bus system. Albeit the increase of system size, the error percentages maintain to be mostly below 5% in the 6716-bus case. This performance guarantee is thanks to the proposed sparse design based on area partitioning, such that the effective complexity for the individual areas stays at the same level. To sum up, the numerical results have well supported the benefits of the proposed GenNN model in

TABLE I: OTS comparisons on the 118-bus system.

	Switching Budget	AC	PWL	DC
Objective	$\alpha = 1$	<b>97.32%</b>	98.10%	99.89%
Cost (%)	$\alpha = 3$	<b>95.23%</b>	96.28%	98.91%
Solver	$\alpha = 1$	<b>0.20%</b>	<b>0.20%</b>	2.10%
Failure (%)	$\alpha = 3$	<b>0.20%</b>	<b>0.20%</b>	2.80%
Constraint	$\alpha = 1$	<b>0.44%</b>	<b>0.44%</b>	1.42%
Violation (%)	$\alpha = 3$	<b>0.44%</b>	0.44%	2.21%
Computation	$\alpha = 1$	52.13 s	4.98 s	<b>3.41 s</b>
Time (s)	$\alpha = 3$	57.67 s	5.89 s	<b>3.89 s</b>

TABLE II: OTS comparisons on the 6716-bus system.

	Switching Budget	PWL	DC
Objective	$\alpha = 1$	<b>99.78%</b>	100.02%
Cost (%)	$\alpha = 3$	<b>98.79%</b>	99.21%
Solver	$\alpha = 1$	<b>2.00%</b>	9.00%
Failure (%)	$\alpha = 3$	<b>4.00%</b>	13.00%
Constraint	$\alpha = 1$	<b>0.27%</b>	0.79%
Violation (%)	$\alpha = 3$	<b>0.27%</b>	1.05%
Computation	$\alpha = 1$	58.36 s	<b>32.80 s</b>
Time (s)	$\alpha = 3$	524.43 s	<b>455.72 s</b>

maintaining power flow relations and improving accuracy, as well as the scalability of the sparse GenNN design in reducing the model complexity and computation burdens. Due to the scalability and high accuracy attained by GenNN\_Sparse, the rest of the simulations will incorporate this model into the topology-related grid optimization tasks.

### B. Applications to the OTS

We implement the proposed GenNN-based PWL-PF model for solving the AC-OTS problem. We will compare it with the DC- and AC-OTS algorithms, both provided by the open-source platform PowerModels.jl [29]. Note that due to the nonconvexity of AC-OTS, the solver therein has adopted the combination of Juniper [30] and interior point optimizer (IPOPT), which may suffer from some sub-optimality issues. Nonetheless, its AC-OTS algorithm could be considered as an excellent baseline for our PWL-based method. To compare across the three OTS methods, we take the line-switching  $\{\epsilon_{ij}\}$  solution from each OTS algorithm's outputs, and fix these topology-related decision variables to re-run the AC-OPF problem using the MATPOWER [31] solver. This way, we can evaluate the performance of the resultant AC-OPF, in terms of the objective costs (for optimality), as well as the percentages of solver failure and constraint violations (for feasibility). We use the objective cost of the AC-OPF problem (with no line-switching flexibility) as the basis to normalize the minimum costs of the OTS methods, and thus the latter will attain the cost percentage below 100%. As for the feasibility, the solver failure metrics measure the rates of the follow-up AC-OPF solver returning an infeasible case, while the constraint violation one depends on the occurrences of operational constraint over-limits for the feasible cases only.



Both metrics can evaluate the quality of the OTS topology solutions in terms of satisfying the operational limits. In addition to these performance metrics, we also compare the computation time for running each of the OTS algorithms excluding the follow-up AC-OPF solution time.

We first compare the three OTS methods for the 118-bus case with Table I listing the four aforementioned metrics. Note that for this table and the other tables, the bold font is used to indicate the best performance in each metric. A switching budget  $\alpha$  of either 1 or 3 is considered. A total of 1,000 PF scenarios by having nodal demands uniformly distributed within [50%, 200%] of the nominal values given in [15] have been generated to compute the average performance. We observe that compared with the AC-OTS, the proposed PWL-OTS approach slightly increases the objective cost by less than 1% while attaining exactly the same feasibility metrics. This competitive optimality-feasibility performance of the PWL-OTS topology decisions strongly confirms the high approximation accuracy of our proposed GenNN model. Meanwhile, the proposed PWL-OTS attains very high computation efficiency, which is in the same order as DC-OTS and takes only a tenth of the AC-OTS's solution time. The DC-OTS unfortunately suffers from a poor feasibility performance due to its lack of PF modeling accuracy.

We also perform the OTS comparisons using the 6716-bus system. For this large system, it becomes impractical to run the AC-OTS algorithm in PowerModels.jl which takes about 40 mins per run. As a result, we compare the proposed PWL-OTS with only DC-OTS, as listed in Table II. Similar to the previous results, the proposed PWL-OTS approach attains a much better performance of optimality and feasibility over DC-OTS. The PWL-OTS's improvements on the feasibility metrics are especially noticeable, thanks to the high approximation accuracy of our proposed GenNN model. Again, its computation complexity is at the same level as the DC-OTS one. All these comparisons have validated the suitability of our GenNN-based PWL power flow model for the topology-optimization task like OTS, as it could approach the near-optimal performance while maintaining a high solution feasibility and low computation complexity.

### C. Applications to the ROP

We utilize the proposed GenNN-based PWL-PF model for solving the AC-ROP problem. We will compare it with the ROP algorithms using the DC- and AC-PF models, both provided by the open-source platform PowerModelsRestoration.jl [32]. Note that similar to the AC-OTS, the AC-ROP algorithm is likely to be sub-optimal but still used here as the baseline for comparisons. To compare across the three ROP methods, we take the solution of restoration order  $\{\epsilon_{ij_i}\}$  for every time  $t \in \mathcal{T}$  from each ROP algorithm's outputs, and fix these decision variables to re-run an AC PF-based optimization problem that intends to maximize the total amount of energy served to customers, as given by

$$\max \quad \sum_{t=1}^T \sum_{i=1}^N x_{i,t} P_{i,t} \quad (17a)$$

$$\text{s.t.} \quad (13b) - (13e). \quad (17b)$$

TABLE III: ROP comparisons on the 118-bus system.

	Damaged Lines	AC	PWL	DC
Energy Served (%)	3	<b>85.3%</b>	83.7%	71.7%
	5	<b>80.1%</b>	75.9%	65.2%
Solver Failure (%)	3	<b>0.20%</b>	<b>0.20%</b>	1.50%
	5	<b>0.40%</b>	0.50%	2.10%
Constraint Violation (%)	3	<b>0.30%</b>	0.37%	2.21%
	5	<b>0.30%</b>	0.44%	2.66%
Computation Time (s)	3	105.12 s	15.36 s	<b>11.41 s</b>
	5	197.67 s	31.34 s	<b>18.83 s</b>

TABLE IV: ROP comparisons on the 6716-bus system.

	Damaged Lines	PWL	DC
Energy Served (%)	3	<b>76.7%</b>	63.3%
	5	<b>68.6%</b>	57.7%
Solver Failure (%)	3	<b>1.00%</b>	6.00%
	5	<b>2.00%</b>	8.00%
Constraint Violation (%)	3	<b>0.05%</b>	0.14%
	5	<b>0.08%</b>	0.23%
Computation Time (s)	3	398.78 s	<b>372.67 s</b>
	5	824.43 s	<b>755.72 s</b>

This way, we can compare the ROP methods based upon the performance in solving the resultant optimization (17), in terms of the energy served (for optimality), as well as solver failure and constraint violations (for feasibility). For the optimality comparison, we compute the percentage of energy served to the customers on the damage-affected buses  $\mathcal{N}^\times \subset \mathcal{N}$  during the restoration, as given by

$$\frac{\sum_{t \in \mathcal{T}} \sum_{i \in \mathcal{N}^\times} x_{i,t} P_{i,t}}{\sum_{t \in \mathcal{T}} \sum_{i \in \mathcal{N}^\times} P_{i,t}}. \quad (18)$$

The higher this percentage is, the better the optimality performance is. As for the feasibility, the solver failure and constraint violation metrics are similar to those considered in the OTS. In addition to these performance metrics, we also compare the computation time for running each of the ROP algorithms.

We first compare the three ROP methods for the 118-bus case with Table III listing the four aforementioned metrics. A restoration budget  $\eta$  of 3 or 5 damaged lines is considered. A total of 1,000 PF scenarios have been similarly generated to compute the average performance. We observe that compared with the AC-ROP, the proposed PWL-ROP approach attains a slightly lower percentage of energy served, yet has almost the same feasibility metrics. This speaks for the competitive optimality-feasibility performance of the PWL-ROP topology decisions and confirms the high approximation accuracy of our proposed GenNN model. Meanwhile, the PWL-ROP algorithm achieves a very high computation efficiency, as it takes only a sixth of the AC-ROP's solution time. Using the same computation complexity to DC-ROP, our proposed PWL-ROP's performance almost approaches the AC-ROP.

We also perform the ROP algorithm comparisons using the 6716-bus system and have to exclude the AC-ROP due to its

very high computational complexity. Table IV lists the comparisons between the proposed PWL-ROP with only the DC-ROP. These large system-based comparisons again confirm the previous observations and verify the PWL-ROP's excellent optimality-feasibility performance improvements over DC-ROP. But yet, the proposed PWL-ROP's computation time is in the same order as the DC-ROP one. Thanks to the high approximation accuracy of our PWL power flow model, it can greatly simplify the computations for multi-period grid topology optimization tasks like ROP while attaining an excellent balance between optimality and feasibility.

## VI. CONCLUSIONS

We developed a data-driven approach for piecewise linear (PWL) PF modeling, using a novel NN layer design with ReLU activation to match the generative structure of AC-PF model. The resulting generative NN (GenNN) models can effectively preserve the consistency among the predicted power variables and integrate the topology decision variables, enabling a mixed-integer linear program (MILP) reformulation for grid topology optimization tasks. We further designed an area-partitioning based sparsification method to reduce the GenNN model complexity. The sparse GenNN models have excellent scalability for large-scale systems, leading to efficient solutions for AC-PF based optimal transmission switching (OTS) and restoration order problems (ROP). Numerical tests on the IEEE 118-bus and the 6716-bus synthetic Texas grid systems have demonstrated the performance improvements of our proposed models in both approximating the AC-PF and expediting topology optimization solutions.

Exciting future directions open up for our GenNN-based linearizable PF models, such as extensions to modeling distribution power flow or carbon emission flow. We can also consider general grid monitoring and operation tasks by accounting for limited sensing and control capabilities. Moreover, implementing the PWL-based grid optimization solutions could benefit from reducing the complexity of the MILP reformulation.

## REFERENCES

- [1] E. B. Fisher, R. P. O'Neill, and M. C. Ferris, "Optimal transmission switching," *IEEE Transactions on Power Systems*, vol. 23, no. 3, pp. 1346–1355, 2008.
- [2] P. Van Hentenryck, C. Coffrin, R. Bent *et al.*, "Vehicle routing for the last mile of power system restoration," in *2011 Power Systems Computation Conference (PSCC)*, 2011.
- [3] B. Stott, J. Jardim, and O. Alsac, "DC power flow revisited," *IEEE Transactions on Power Systems*, vol. 24, no. 3, pp. 1290–1300, 2009.
- [4] C. Coffrin and P. Van Hentenryck, "A linear-programming approximation of AC power flows," *INFORMS Journal on Computing*, vol. 26, no. 4, pp. 718–734, 2014.
- [5] P. A. Trodden, W. A. Bukhsh, A. Grothey, and K. I. McKinnon, "Optimization-based islanding of power networks using piecewise linear AC power flow," *IEEE Transactions on Power Systems*, vol. 29, no. 3, pp. 1212–1220, 2013.
- [6] W. E. Brown and E. Moreno-Centeno, "Transmission-line switching for load shed prevention via an accelerated linear programming approximation of AC power flows," *IEEE Transactions on Power Systems*, vol. 35, no. 4, pp. 2575–2585, 2020.
- [7] Y. Liu, N. Zhang, Y. Wang, J. Yang, and C. Kang, "Data-driven power flow linearization: A regression approach," *IEEE Transactions on Smart Grid*, vol. 10, no. 3, pp. 2569–2580, 2018.
- [8] M. Jia and G. Hug, "Overview of data-driven power flow linearization," in *2023 IEEE Belgrade PowerTech*. IEEE, 2023, pp. 01–06.
- [9] J. Chen, W. Wu, and L. A. Roald, "Data-driven piecewise linearization for distribution three-phase stochastic power flow," *IEEE Transactions on Smart Grid*, vol. 13, no. 2, pp. 1035–1048, 2021.
- [10] A. Kody, S. Chevalier, S. Chatzivasileiadis, and D. Molzahn, "Modeling the AC power flow equations with optimally compact neural networks: Application to unit commitment," in *2022 Power Systems Computation Conference (PSCC)*, 2022.
- [11] G. Chen, H. Zhang, and Y. Song, "Efficient constraint learning for data-driven active distribution network operation," *IEEE Transactions on Power Systems*, 2023.
- [12] L. Sang, Y. Xu, and H. Sun, "Encoding carbon emission flow in energy management: A compact constraint learning approach," *IEEE Transactions on Sustainable Energy*, 2023.
- [13] B. Huang and J. Wang, "Applications of physics-informed neural networks in power systems—a review," *IEEE Transactions on Power Systems*, vol. 38, no. 1, pp. 572–588, 2022.
- [14] J. Jalving, M. Eydenberg, L. Blakely, A. Castillo, Z. Kilwein, J. K. Skolfield, F. Boukouvala, and C. Laird, "Physics-informed machine learning with optimization-based guarantees: Applications to AC power flow," *International Journal of Electrical Power & Energy Systems*, vol. 157, p. 109741, 2024.
- [15] [Online]. Available: <http://labs.ece.uw.edu/pstca/>
- [16] C. Mateo, F. Postigo, T. Elgindy, A. B. Birchfield, P. Dueñas, B. Palmintier, N. Panossian, T. Gómez, F. de Cuadra, T. J. Overbye *et al.*, "Building and validating a Large-scale combined transmission & distribution synthetic electricity system of Texas," *International Journal of Electrical Power & Energy Systems*, vol. 159, p. 110037, 2024.
- [17] M. Bazrafshan, N. Gatsis, and H. Zhu, "Optimal tap selection of step-voltage regulators in multi-phase distribution networks," in *2018 Power Systems Computation Conference (PSCC)*. IEEE, 2018, pp. 1–7.
- [18] J. W. Simpson-Porco, "A theory of solvability for lossless power flow equations—Part I: Fixed-point power flow," *IEEE Transactions on Control of Network Systems*, vol. 5, no. 3, pp. 1361–1372, 2017.
- [19] G. V. Trunk, "A problem of dimensionality: A simple example," *IEEE Transactions on pattern analysis and machine intelligence*, no. 3, pp. 306–307, 1979.
- [20] A. B. Birchfield, K. M. Gegner, T. Xu, K. S. Shetye, and T. J. Overbye, "Statistical considerations in the creation of realistic synthetic power grids for geomagnetic disturbance studies," *IEEE Transactions on Power Systems*, vol. 32, no. 2, pp. 1502–1510, 2016.
- [21] A. Ng, M. Jordan, and Y. Weiss, "On spectral clustering: Analysis and an algorithm," *Advances in neural information processing systems*, vol. 14, 2001.
- [22] R. J. Sánchez-García, M. Fennelly, S. Norris, N. Wright, G. Niblo, J. Brodzki, and J. W. Bialek, "Hierarchical spectral clustering of power grids," *IEEE Transactions on Power Systems*, vol. 29, no. 5, pp. 2229–2237, 2014.
- [23] H. Zhu and G. B. Giannakis, "Sparse overcomplete representations for efficient identification of power line outages," *IEEE Transactions on Power Systems*, vol. 27, no. 4, pp. 2215–2224, 2012.
- [24] I. Griva, S. G. Nash, and A. Sofer, *Linear and nonlinear optimization*. Siam, 2009, vol. 108.
- [25] S. Fattahi, J. Lavaei, and A. Atamtürk, "A bound strengthening method for optimal transmission switching in power systems," *IEEE Transactions on Power Systems*, vol. 34, no. 1, pp. 280–291, 2018.
- [26] R. Anderson, J. Huchette, W. Ma, C. Tjandraatmadja, and J. P. Vielma, "Strong mixed-integer programming formulations for trained neural networks," *Mathematical Programming*, vol. 183, no. 1, pp. 3–39, 2020.
- [27] W. E. Hart, J.-P. Watson, and D. L. Woodruff, "Pyomo: modeling and solving mathematical programs in python," *Mathematical Programming Computation*, vol. 3, no. 3, pp. 219–260, 2011.
- [28] Gurobi Optimization, LLC, "Gurobi Optimizer Reference Manual," 2023. [Online]. Available: <https://www.gurobi.com>
- [29] C. Coffrin, R. Bent, K. Sundar, Y. Ng, and M. Lubin, "Powermodels.jl: An open-source framework for exploring power flow formulations," in *2018 Power Systems Computation Conference (PSCC)*, 2018.
- [30] O. Kröger, C. Coffrin, H. Hijazi, and H. Nagarajan, "Juniper: An Open-Source Nonlinear Branch-and-Bound Solver in Julia," in *Integration of Constraint Programming, Artificial Intelligence, and Operations Research*. Springer International Publishing, 2018, pp. 377–386.
- [31] R. D. Zimmerman, C. E. Murillo-Sánchez, and R. J. Thomas, "MATPOWER: Steady-state operations, planning, and analysis tools for power systems research and education," *IEEE Transactions on power systems*, vol. 26, no. 1, pp. 12–19, 2010.
- [32] N. Rhodes, D. M. Fobes, C. Coffrin, and L. Roald, "Powermodel-restoration.jl: An open-source framework for exploring power network

restoration algorithms,” in *2020 Power Systems Computation Conference (PSCC)*, June 2020.